Thermoelectric Properties of Highly Conductive Poly(3,4-ethylenedioxythiophene) Polystyrene Sulfonate Printed Thin Films

Davide Beretta,[†,‡] Alex J. Barker,[†] Isis Maqueira-Albo,[†,‡] Alberto Calloni,[‡] Gianlorenzo Bussetti,[‡] Giorgio Dell'Erba,[†] Alessandro Luzio,[†] Lamberto Duò,[‡] Annamaria Petrozza,[†] Guglielmo Lanzani,[†,‡] and Mario Caironi*[,†]

[†]Center for Nano Science and Technology @PoliMi, Istituto Italiano di Tecnologia, via Pascoli 70/3, 20133 Milano (MI), Italy
[‡]Dipartimento di Fisica, Politecnico di Milano, P.zza Leonardo da Vinci 32, 20133 Milano (MI), Italy

ABSTRACT: Organic conductors are being evaluated for potential use in waste heat recovery through lightweight and flexible thermoelectric generators manufactured using cost-effective printing processes. Assessment of the potentiality of organic materials in real devices still requires a deeper understanding of the physics behind their thermoelectric properties, which can pave the way toward further development of the field. This article reports a detailed thermoelectric study of a set of highly conducting inkjet-printed films of commercially available poly(3,4-ethylenedioxythiophene) polystyrene sulfonate formulations characterized by in-plane electrical conductivity, spanning the interval 10−500 S/cm.
The power factor is maximized for the formulation showing an intermediate electrical conductivity. The Seebeck coefficient is studied in the framework of Mott's relation, assuming a (semi-)classical definition of the transport function. Ultraviolet photoelectron spectroscopy at the Fermi level clearly indicates that the shape of the density of states alone is not sufficient to explain the observed Seebeck coefficient, suggesting that carrier mobility is important in determining both the electrical conductivity and thermopower. Finally, the cross-plane thermal conductivity is reliably extracted thanks to a scaling approach that can be easily performed using typical pump-probe spectroscopy.

KEYWORDS: thermoelectric, Seebeck, thermopower, organic conductors, organic thermoelectrics, power factor, PEDOT:PSS

INTRODUCTION

The thermoelectric effect encompasses a set of phenomena enabling direct conversion between thermal and electrical energy. The efficiency of devices based on the thermoelectric effect depends on many parameters, among which the thermoelectric properties of the constituent matter play a fundamental role. These are summarized in the dimensionless figure of merit[1]

$$zT = \frac{\sigma\alpha^2}{\kappa}T \quad (1)$$

where T is the absolute temperature, σ is the electrical conductivity, α is the thermopower (or Seebeck coefficient), and $\kappa = \kappa_{el} + \kappa_{ph}$ is the thermal conductivity; the latter is given by the sum of the electronic κ_{el} and phonon κ_{ph} contributions. The higher the figure of merit, the higher the conversion efficiency of thermoelectric devices. Therefore, the ideal thermoelectric material is a perfect thermal insulator and an excellent electrical conductor (phonon-glass electron-crystal), with a high thermopower. Unfortunately, these conditions are hardly obtained: generally, increasing the electrical conductivity by doping results in a simultaneous increase in the thermal conductivity (mediated by charge carriers) and a decrease in the thermopower.[1,2]

Many solutions were proposed to decouple the transport properties entering the figure of merit and thus to overcome the limitations arising from such interrelations. Among them, two general methodologies are distinguished, namely (i) increasing the power factor, PF = $\sigma\alpha^2$, and (ii) decreasing the phonon contribution to the thermal conductivity. To this extent, nanostructures, nanocomposites, and complex materials (such as skutterudites, clathrates, and half-Heusler) have been identified as the most promising paths.[3−6] Among the wide panorama of materials studied, conducting polymers are receiving increasing attention in the thermoelectric community as potential materials to address a variety of novel applications that require flexibility and/or adaptability to curved surfaces, which can be targeted through devices realized by cost-effective processes such as printing.[7−12] The intrinsic disordered nature of conducting polymers is responsible for the relatively low phonon contribution to their thermal conductivity. This has motivated efforts to improve their power factor, rather than reduce thermal conductivity, as a route toward improvement of their thermo-

electric properties.[13] Starting from there, many efforts have been spent in the controlled doping of semiconducting polymers. Whereas in most of the cases, as expected from theory, doping was observed to induce the reduction of thermopower,[14−18] simultaneous enhancement of electrical conductivity and thermopower was shown possible for a family of conducting polymers, depending on the doping mechanism and by postprocessing treatment.[19,20] The possibility of simultaneous enhancement of the two thermoelectric coefficients suggests the need of a detailed investigation of the transport properties of conducting polymers, with the aim to identify the physics determining the correlations between the thermoelectric coefficients. Among the conjugated conducting polymers, doped poly(3,4-ethylenedioxythiophene) (PEDOT) is one of the most studied.[21] Understanding its thermoelectric properties represents a key step for the design and synthesis of more performing thermoelectric polymers. The best reported thermoelectric parameters for PEDOT were obtained upon doping in the presence of tosylate counterions (PEDOT:Tos) following an in situ chemical or vapor-phase polymerization.[8,20,22,23] On the other hand, soluble and printable formulations of PEDOT that are doped in the presence of polysterene sulfonate (PSS) counterions (PEDOT:PSS) have been developed for a long time and are commercially available. In the last two decades, many studies have been devoted to investigating the effect of temperature and solvents on the transport properties and mechanisms of thin and thick films of PEDOT:PSS, which were found to be strongly anisotropic with respect to the plane of growth[23−27] and highly sensitive to solvents and postprocessing treatments affecting the morphology of the film.[28−32] In particular, the cross-plane electrical conductivity is generally two orders of magnitude lower than the corresponding in-plane value.[24,25] This effect could be ascribed to the preferential in-plane orientation of the polymer chains, which possibly leads to smaller mobility in the cross-plane direction and thus anisotropic electrical conductivity.[25] Likewise, the in-plane thermal conductivity $\kappa_{\parallel}$ of thin films was found to be dependent on charge-carrier density in agreement with the Wiedemann−Franz law, whereas evidence for the validity of such relation for the cross-plane thermal conductivity $\kappa_{\perp}$ has not been given yet.[26]

Since the density of states, $n(\varepsilon)$, features in the definition of thermoelectric coefficients, detailed studies on how the Seebeck coefficient and electrical and thermal conductivity vary as a function of $n(\varepsilon)$ are beneficial in developing a solid understanding of the physics governing PEDOT:PSS and organic thermoelectrics in general. However, so far there are only limited examples in this direction.[20,33,34] In particular, attempts to correlate the shape of $n(\varepsilon)$ at the Fermi level with the Seebeck coefficient, which are interdependent in degenerate systems according to Mott's relation (see eq 3 below),[35] have previously been done using ultraviolet photoelectron spectroscopy (UPS) assuming a (semi-)classical picture of the transport function $\sigma(\varepsilon) = q\mu(\varepsilon)\, n(\varepsilon)$, where $\mu(\varepsilon)$ is the energy mobility function and q is the unit charge carrier, and under assumption that $\mu(\varepsilon)$ saturates to a maximum level above a certain degree of oxidation.[36]

This work reports a detailed thermoelectric study of a set of highly conducting inkjet-printed films of commercially available PEDOT:PSS characterized by different electrical conductivities, namely Orgacon ICP1050, Clevios PJ700, and Orgacon IJ1005. The transport mechanism is first investigated by studying the temperature dependence of the electrical conductivity and Seebeck coefficient. The power factor is maximized for the formulation showing an intermediate electrical conductivity. Given the linear temperature dependence of α found for each formulation, the systems can be assumed to be degenerate and thus studied in the framework of Mott's relation. Assuming a (semi-)classical picture for the transport function, UPS spectra at the Fermi level are acquired with the aim to identify direct correlations between the Seebeck coefficient and the shape of the density of states at the conduction level. The shapes of $n(\varepsilon)$ at the Fermi level are found to be insufficient on their own to explain the differences among the measured thermopowers, clearly indicating that the dependence of the Seebeck coefficient on charge-carrier mobility cannot be neglected for these thermoelectric systems. Finally, the cross-plane thermal conductivity is reliably extracted thanks to a scaling approach that can be easily performed using typical pump−probe spectroscopy without resorting to more complicated phase-sensitive techniques, providing the basis for a first estimate of the in-plane dimensionless figure of merit $z_{\parallel}T$ under simple hypotheses which find agreement in previous measurements.

EXPERIMENTAL METHODS

Three different commercially available PEDOT:PSS formulations, namely, Orgacon ICP1050, Clevios PJ700, and Orgacon IJ1005, were purchased from Sigma Aldrich and used as received. Samples for the in-plane power factor characterization were prepared by depositing 5 mm large and 50 mm long PEDOT:PSS stripes on Kapton (DuPont) by inkjet printing (FujiFilm Dimatix DMP-2831, 10 pL of droplet volume). More than 10 layers were deposited to achieve a thickness of approximately 0.5 μm. Since the profile of the films was found to be characterized by thickness variation in the order of 10−20%, sample thickness was evaluated as an average value over the whole sample width. The stripes were then cut into 12 mm long samples and annealed at 373 K for 1 h in air to promote water desorption. Au stripes (50 nm thick) were subsequently deposited by thermal evaporation at the two ends of the sample to improve the electrical contact between the sample and the thermocouples employed for measurement of the power factor. Au stripes were grown perpendicular to the direction of the thermal gradient induced during the measurement so that misalignments do not influence the measurement of the temperature gradient and thus the measured thermoelectric properties of the films. Finally, a second thermal annealing at 453 K for 30 min was performed directly under vacuum in the system used for the measurement of the power factor. This second annealing performed at a temperature higher than the maximum temperature of measurement was effective in removing any hysteretic effects that could arise during the measurement due to water molecule absorption/desorption. The in-plane thermopower $\alpha_{\parallel}$ and the in-plane electrical conductivity $\sigma_{\parallel}$ were measured using an improved homemade system previously developed by some of the authors and validated on reference Nickel samples.[37] The system is now also capable of measuring the electrical conductivity with a double-scan method: from room temperature down to ≅260 K, up to ≅420 K, and finally back to the room temperature, with steps of 20 K. This measurement method was chosen to reveal eventual hysteretic effects and to verify the thermal stability of the PEDOT:PSS under vacuum. A scheme of the measurement method is shown in Figure 1a: the thermopower is measured by inducing a temperature difference, ΔT, increasing with time on the sample; ΔT and the corresponding voltage generated, V, are recorded as a function of time, and according to the methodology discussed by Beretta et al.[37] the thermopower is calculated as $\alpha(T) = \alpha_{\mathrm{Cu}}(T) - \left.\frac{\mathrm{d}V}{\mathrm{d}\Delta T}\right|_{\Delta T=0}$, where $\alpha_{\mathrm{Cu}}(T)$ is the thermopower of copper evaluated at temperature T. The electrical conductivity is calculated for isothermal samples, with a four-collinear-probes method by forcing a current I in the sample and measuring the voltage drop V. From a data set corresponding to different current values, and once the geometrical dimensions of the samples are known, the conductivity is extracted as $\sigma = \frac{l}{S}\frac{\mathrm{d}I}{\mathrm{d}V}$, where l and S are the length and section of the sample, respectively. The characterization of the electrical conductivity

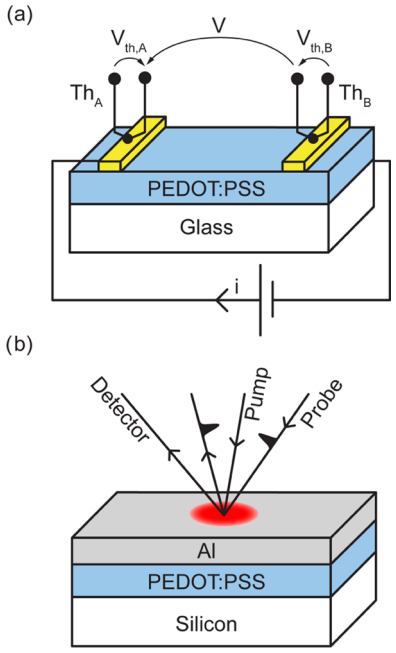

Figure 1. a) Scheme of the measurement method of the power factor. T-type thermocouples (copper–constantan) are used to probe the temperature of the samples in A and B, whereas their copper wires are used to measure the voltage, *V*, developed due to the Seebeck effect. (b) Scheme of measurement of the cross-plane thermal conductivity by the pump–probe method. If the characteristic dimension of the laser spot is much larger than the thickness of the film, the heat transport parallel to the aluminum film surface can be neglected, and the problem can be treated as one-dimensional (1D).

and the thermopower at room temperature was performed on a batch of seven samples per type, whereas only two samples per type were chosen and studied in the whole temperature range.

X-ray photoelectron spectroscopy (XPS) and UPS characterizations were performed on two samples per material type, realized by inkjet printing (FujiFilm Dimatix DMP-2831, 10 pL of droplet volume) on 1 × 1 cm^2 × 0.7 mm Corning glass substrates previously coated by 30 nm of Au, the latter being deposited by thermal evaporation. To be consistent with the thermoelectric characterization, the samples were annealed at 453 K for 30 min under vacuum, in the same system used for the XPS and UPS characterizations described in the work of Berti et al.[38] Unmonochromatized Mg Kα radiation ($h\nu$ = 1253.6 eV) and He I radiation ($h\nu$ = 21.2 eV) were used for XPS and UPS, respectively. Photoemission spectra were acquired using a hemispherical analyzer working at a pass energy of 20 eV (1.5 eV) for XPS (UPS), resulting in an overall full width at half-maximum (FWHM) resolution of about 0.9 eV (50 meV). Source satellites were always subtracted. All measurements were acquired at normal emission, with the sample kept at room temperature. To exclude any appreciable differences in the transport properties of samples prepared on Kapton and glass substrates and thus confirm the consistency of the photoelectron spectroscopy measurements with the thermoelectric transport ones, samples for thermoelectric characterization were also prepared on glass. Measurements (not shown) reveal no differences in the Seebeck coefficient nor in the electrical conductivity.

The cross-plane thermal conductivity, $\kappa_\perp$, was measured using an optical pump–probe technique, a scheme of which is shown in Figure 1b, on the basis of a method developed by Capinski and co-workers.[39] Unlike the phase-sensitive implementations of time-domain thermoreflectance,[40] this method can be easily performed using typical pump–probe spectroscopy setups. Additionally, the system implemented is capable of measuring thermal decays over very long pump–probe delays (100 fs to 1 ms), enabling measurement of films with a wide range of thicknesses. One drawback is the inability to simultaneously determine heat capacity, although this can be measured by other techniques, such as differential scanning calorimetry. Thin films of each polymer were coated on silicon substrates, previously treated with oxygen plasma, by multiple spin coating to obtain a thickness in the 100–400 nm range. Inkjet printing is not viable in this case because a very high uniformity and smoothness of the surface is required. The samples were then annealed for 30 min at 400 K to promote solvent desorption. Finally, a highly reflective, thin (80–90 nm), and very uniform layer of aluminum was deposited by thermal evaporation on top of the polymer. In this experiment, a pulse from a Q-switched Nd:YVO_4 laser (532 nm, 700 ps FWHM pulse width, 350 μm FWHM spot size) creates a transient increase in the temperature of the aluminum, which then cools by transferring heat through the polymer sample into the silicon substrate. This temperature increase, $\Delta T(t)$, results in a change in reflectivity $\Delta R(t)$, which can be monitored by an optical probe pulse. The fundamental output of an amplified Ti:sapphire laser (800 nm, 150 fs FWHM) was used to generate probe pulses, which were synchronized with the Q-switched pump laser via a digital delay generator enabling to resolve temperature changes from 1 ns to 1 ms and were detected using a silicon photodiode and lock-in amplifier. Measurements conducted using the Ti:sapphire source as both the pump and the probe (with a mechanical delay stage, time resolution ~200 fs) confirmed that negligible cooling occurs within the first nanosecond for the samples in this study. The relatively slow repetition rate of the system (1 kHz) allowed complete cooling of the samples between pulses, such that heat accumulation or (equivalently) out-of-phase contributions to the lock-in signal did not need to be considered. As the pump laser spot size is much larger than the thickness of the polymer–aluminum stack, cooling of the sample is well modeled as a 1D problem, in which the heat transfer at each interface is characterized by an interfacial thermal (Kapitza) conductance. Knowledge of the bulk thermal characteristics of the materials studied leaves only three free parameters for the model: out-of-plane thermal conductivity of the polymer $\kappa_\perp$ and Kapitza thermal conductance of each of the interfaces ($K_{Al/PEDOT:PSS}$ and $K_{PEDOT:PSS/Si}$). By simultaneously fitting data from several samples varying only the polymer thickness, the model correctly predicts the thickness dependence of cooling and ensures a unique solution to the fit. The fitting results are sensitive to aluminum thermal properties and PEDOT:PSS heat capacity and only weakly sensitive to silicon thermal properties. The parameters used in this work are reported in Table 1, in which a single heat capacity value taken from the literature is used for every PEDOT:PSS sample.[26]

Table 1. Thermal Properties of Aluminum, Silicon, and PEDOT:PSS Used in This Work for the Estimation of the Thermal Conductivity of PEDOT:PSS by Pump–Probe Method

	κ (W m^{-1} K^{-1})	C_v (J m^{-3} K^{-1})
aluminum[41]	237	2.1×10^6
silicon[41,42]	140	1.9×10^6
PEDOT:PSS[26]		1.5×10^6

RESULTS AND DISCUSSION

Three commercially available solutions of PEDOT:PSS, namely, ICP1050, PJ700, and IJ1005, characterized by different electrical conductivities and selected on the basis of their processability using inkjet printing, were studied with the aim of assessing their thermoelectric properties in view of future cost-effective fabrication of plastic thermoelectric generators. In detail, PJ700 and IJ1005 are highly conducting inks specifically formulated for inkjet, whereas ICP1050 is a formulation with a nominally lower conduction for which printability was assessed in the framework of this work. A comparative XPS elemental analysis of inkjet-printed films was first carried out to characterize the chemical composition of the as-processed formulations. The results of

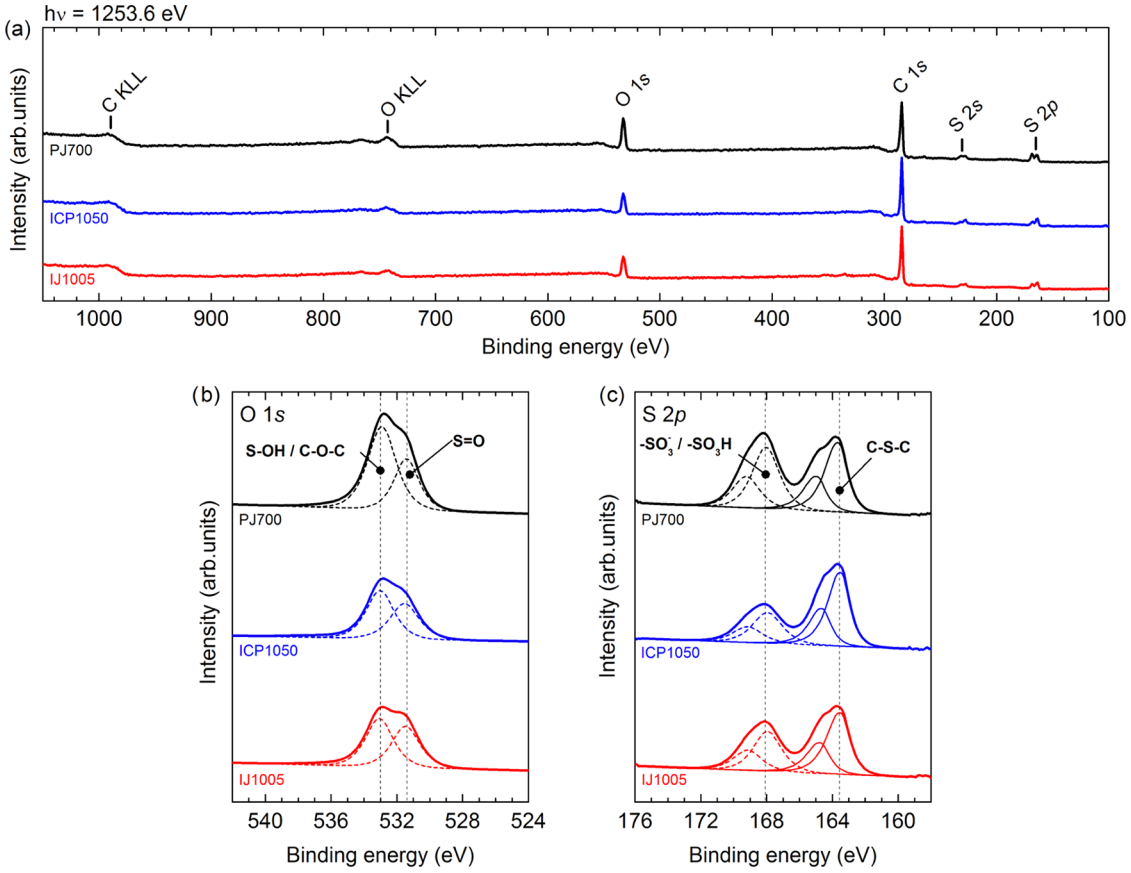

Figure 2. (a) XPS wide scans from representative PJ700, ICP1050, and IJ1005 samples. To circumvent any possible charging artifact related to the different conductivities of the three samples, all spectra are reported by adjusting the binding energy (BE) scale to set the photoemission signal from the C 1*s* core level at a BE of 285.0 eV, following the methodology of Greczynski et al.[46] (b, c) detailed scans of the O 1*s* and S 2*p* regions, respectively. The O 1*s* spectra are reproduced by means of two symmetric line shapes centered at a BE of about 532.1 eV (oxygen atoms in sulfonic acid, S═O bond) and 533.6 eV (oxygen in hydroxyl groups and in the PEDOT ethylene bridge, −OH and C−O−C bonds, respectively). Photoemission from the S 2*p* level gives rise to a spin-orbit split doublet, with a BE difference between the S $2p_{1/2}$ and S $2p_{3/2}$ peaks of 1.18 eV and an intensity ratio of 1:2.[45,46] The sulfur region is characterized by the presence of the photoemission signal from S atoms in the thiophene rings and in the sulfonic acid groups, which is characteristic of PEDOT and PSS, respectively.[45,46] PEDOT (PSS) contributes to the doublet at the lower (higher) BE [S $2p_{3/2}$ peak at about 164.1 eV (168.6 eV)].

such analysis are shown in Figure 2. XPS measurements reveal spectroscopic features related to the presence of oxygen, carbon, and sulfur, as expected from the chemical composition of the polymers, whereas no significant contribution from other chemical species, possibly derived from different additives, is observed. Therefore, despite the depth probed by our XPS characterization is limited to a thin layer of a few nanometers from the sample surface,[43] compared to an overall film thickness of about 500 nm, the chemical composition of the solid-state printed films obtained from the three commercial formulations can be considered equivalent.

The relative content of PEDOT and PSS can strongly influence the electronic properties of the printed films.[44] The fractional amount of PSS ($w_{\%}^{PSS}$) has been estimated by considering the relative intensities of the photoemission signals from the sulfur atoms ($I_{S\ 2p}$) in the thiophene rings and in the sulfonic acid groups, characteristic of PEDOT and PSS, respectively.[45] Because both PEDOT and PSS feature a single S atom per monomeric unit, $w_{\%}^{PSS}$ can be calculated according to

$$w_{\%}^{PSS} = 100 \times \frac{I_{S\ 2p}^{PSS}}{I_{S\ 2p}^{PEDOT} + I_{S\ 2p}^{PSS}} \quad (2)$$

The fractional amount of PSS is found to be different among the studied PEDOT:PSS formulations, spanning the interval 35−52%, as shown in Figure 3. However, the PSS content analysis does not provide a direct correlation between the relative PSS content and the room-temperature electrical conductivity, which

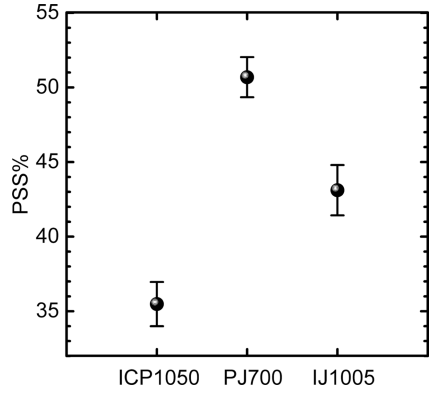

Figure 3. Fractional amount of PSS measured from the relative intensities of the S 2*p* doublets shown in Figure 2c. Error bars account for uncertainties arising from the fitting procedure.

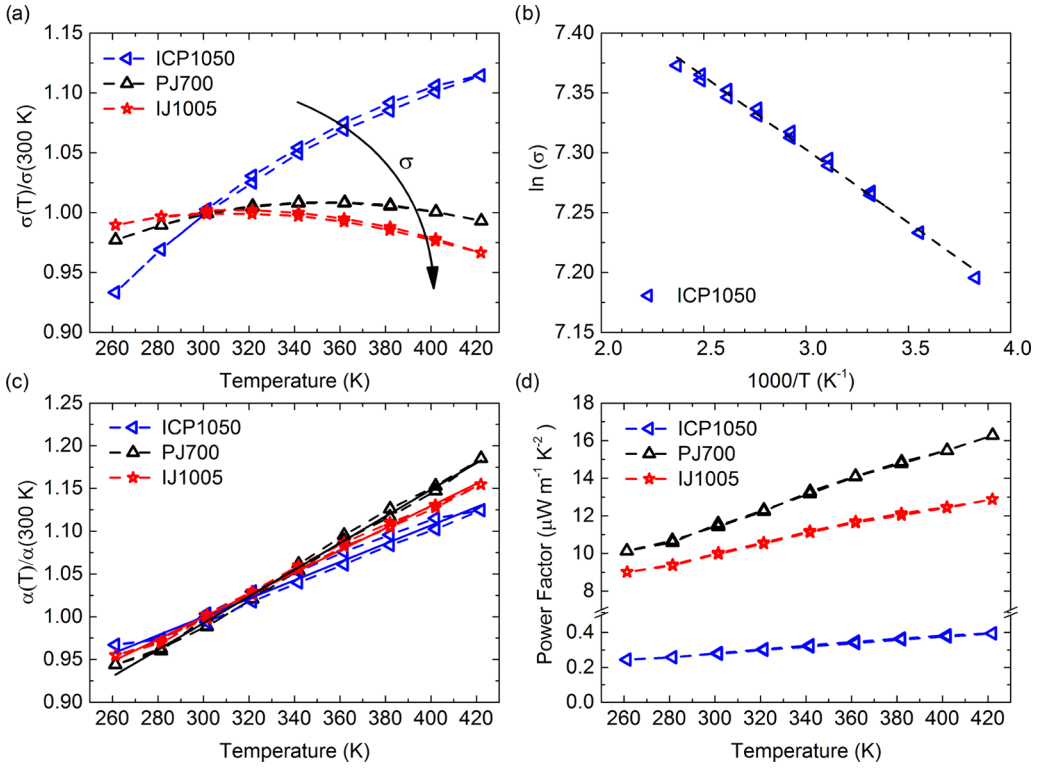

Figure 4. a) Electrical conductivity normalized with respect to room-temperature values. The transport mechanism is thermally activated in the whole temperature range for the less conductive PEDOT:PSS, namely ICP1050, whereas it reveals a metal-like transport mechanism above a certain temperature for the most conductive ones, namely, PJ700 and IJ1005. (b) Arrhenius plot of a representative sample of the ICP1050 batch and its linear fit. (c) Thermopower normalized with respect to room-temperature values. $\alpha_{\parallel}(T)$ is a linear function of temperature for each type of PEDOT:PSS studied regardless of the transport mechanism. (d) Power factor of representative samples of PEDOT:PSS. All of the curves are obtained from a double sweep measurement: from room temperature to low temperature, up to high temperature and then back to room temperature again.

Table 2. $\sigma_{\parallel}(T)$, $\alpha_{\parallel}(T)$, $PF_{\parallel}(T)$, and $\kappa_{\perp}(T)$ at Room Temperature of the Three Formulations of PEDOT:PSS Studied[a]

	$\sigma_{\parallel}$ (S cm^{-1})	$\alpha_{\parallel}$ (μV K^{-1})	$PF_{\parallel}$ (μW m^{-1} K^{-2})	$\kappa_{\perp}$ (W m^{-1} K^{-1})
ICP1050	11.32 ± 1.57	14.31 ± 1.03	0.23 ± 0.05	0.34
PJ700	267.12 ± 4.05	21.42 ± 0.36	12.26 ± 0.45	0.45
IJ1005	462.86 ± 4.39	14.48 ± 0.32	9.70 ± 0.37	0.46

[a] $\sigma_{\parallel}(T)$, $\alpha_{\parallel}(T)$, and $PF_{\parallel}(T)$ were evaluated as an average over a batch of seven samples per type, whereas $\kappa_{\perp}(T)$ was estimated by fitting several samples characterized by different thicknesses, assuming that the thermodynamic properties and the interfacial thermal resistances are thickness-independent.

should find its explanation in the fine nanostructure of the films, the characterization of which is beyond the scope of this work. Atomic force microscopy (AFM) topography images (reported in the Supporting Information) reveal a smooth surface in all cases: while printed films of ICP1050 and IJ1005 show a root-mean-square roughness of ~0.7–0.8 nm, printed films of PJ700, that is, the formulation with the highest PSS content, show a higher roughness of 1.7 nm.

The in-plane electrical conductivity $\sigma_{\parallel}$ of the printed films, measured at room temperature and averaged over a batch of seven samples per formulation, is equal to 11.32 ± 1.57, 267.12 ± 4.05, and 462.86 ± 4.39 S/cm for ICP1050, PJ700, and IJ1005, respectively, scaling in agreement with the nominal values. The normalized temperature-dependent electrical conductivity, $\sigma_{\parallel}(T)/\sigma_{\parallel}(300\ \mathrm{K})$, evaluated in the temperature range 260–420 K for representative samples is shown in Figure 4a. Despite the very small variation of the electrical conductivities in the temperature range investigated, namely within ±10% of room-temperature values, the different functional shapes of $\sigma_{\parallel}(T)$ are clearly distinguishable and reproduced in a double scan measurement method. In particular, while the less conductive formulation (ICP1050) shows a thermally activated hopping transport mechanism across the full temperature range, the more conductive samples (PJ700 and IJ1005) reveal a transition to a metal-like transport mechanism (i.e., $d\sigma/dT < 0$) above a certain value of temperature. More precisely, $\sigma_{\parallel}(T)$ becomes a decreasing function of temperature approximately above 360 and 320 K for PJ700 and IJ1005, respectively. The electrical conductivity of ICP1050 can be described by a thermally activated process, indicating a hopping transport regime according to[47]

$$\sigma_{\parallel}(T) = \sigma_{\parallel,0} \exp\left(-\frac{W}{k_B T}\right) \tag{3}$$

where W is the activation energy and k_B is the Boltzmann constant. The Arrhenius plot of a representative sample taken from the ICP1050 batch is shown in Figure 4b, from which the activation energy of ICP1050 is found to be W = 11.4 meV.

The in-plane thermopower $\alpha_{\parallel}(T)$ was measured in the same temperature range as the electrical conductivity. Measurements at room temperature, averaged over a batch of seven samples per formulation, gave 14.31 ± 1.03, 21.42 ± 0.36, and 14.48 ± 0.32 μV/K for ICP1050, PJ700, and IJ1005, respectively. Results of the temperature-dependent measurements taken on representative samples and normalized with respect to room-temperature values are shown in Figure 4c. The in-plane thermopower is found to be linearly dependent on temperature for all of the samples, regardless of whether their characteristic electron transport mechanism is thermally activated or not. This is a trend generally observed in degenerate systems.[2,48] As a result of the functional shapes of electrical conductivity and thermopower, the in-plane power factor, $PF_{\parallel}$, follows a quasilinear trend with temperature and reaches its maximum at higher temperatures. Room-temperature values that are averaged over a batch of seven samples per formulation are reported in Table 2. The characterization demonstrates that the highest power factor is obtained as a trade-off between the electrical conductivity and the thermopower, achieving the maximum value of 12.26 ± 0.45 μW m^{-1} K^{-2} in the samples featuring an intermediate value of electrical conductivity.

The thermoelectric characterization was completed by the measurement of the cross-plane thermal conductivity, $\kappa_{\perp}$, at room temperature, using a simplified spectroscopic approach described in the Experimental Methods and by the estimation of the in-plane thermal conductivity, $\kappa_{\parallel}$, by means of simple considerations, which find basis in previous measurements. In Figure 5a, the variation of reflectivity, ΔR, of the aluminum deposited on top of the films is shown with respect to time for three samples of IJ1005, characterized by a different thickness. The experimental data (open circles) are fitted (solid lines) considering 1D heat diffusion through the bulk of the three layers (aluminum, polymer, and silicon substrate) and through each interface, characterized by an interfacial thermal (Kapitza) conductance, with the same parameters of interfacial thermal resistance and material properties for each polymer thickness studied.

The fitting curves reproduce the experimental data very well. The cross-plane thermal conductivity, reported in Table 2, is found to increase from the least electrically conductive sample to the most conductive, this increment being on the order of 35%. The cross-plane thermal conductivity is plotted with respect to the in-plane electrical conductivity in Figure 5b, and data are compared with that observed by Liu et al. for drop-cast films.[26] Although we could not measure the cross-plane electrical conductivity, $\sigma_{\perp}$, this is expected to vary among the formulations studied, given the large variation observed in $\sigma_{\parallel}$. Taking into account the well-known anisotropic transport properties of PEDOT:PSS,[25,27] the variation observed in the cross-plane thermal conductivity from the least to the most electrically conducting sample can be explained as due to the electronic contribution, $\kappa_{\perp,el}$, by means of the Wiedemann−Franz law only if $\sigma_{\perp}$ is in the same order as that of $\sigma_{\parallel}$. On the other hand, if $\sigma_{\perp}/\sigma_{\parallel} < 10^{-1}$, where $\kappa_{\perp,el}$ is negligible, then the variation observed in the cross-plane thermal conductivity must be ascribed to the phonon contribution, $\kappa_{\perp,ph}$. Therefore, without a direct measurement of $\sigma_{\perp}$, the validity of the Wiedemann−Franz law in the cross-plane direction cannot be excluded a priori. However, previous studies typically report an anisotropy factor of the electrical conductivity in the order of $\sigma_{\perp}/\sigma_{\parallel} \sim 10^{-2}$.[25] By assuming a similar factor in the present case, $\kappa_{\perp,el}$ would be negligible, and a legitimate first order estimation of the in-plane thermal conductivity, $\kappa_{\parallel}$, can be

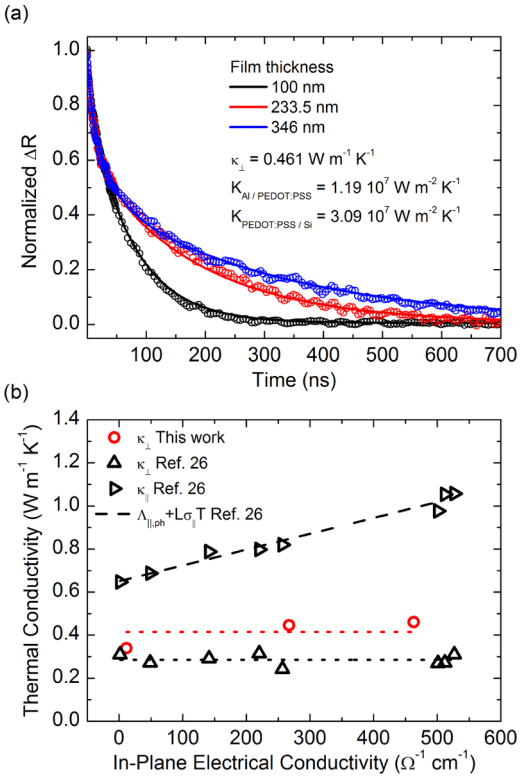

Figure 5. (a) Normalized reflectivity variation with time of the aluminum film for the IJ1005 samples. The cross-plane thermal conductivity is extracted from the fitting of a series of films with different thickness. (b) In-plane and cross-plane thermal conductivities plotted as functions of the in-plane thermal conductivity. The red circles represent data measured in this work.

obtained as $\kappa_{\parallel} = \kappa_{\parallel,ph} + \kappa_{\parallel,el}$, where $\kappa_{\parallel,ph} \cong 2\kappa_{\perp,ph}$ and $\kappa_{\parallel,el} = \sigma_{\parallel}LT$, with $L = 2.44 \times 10^{-8}$ W Ω K^{-2}, the Lorenz number, as previously observed in similar systems.[26] Accordingly, on an average, we obtain $\kappa_{\parallel}^{ICP1050} \cong 0.69$ W m^{-1} K^{-1}, $\kappa_{\parallel}^{PJ700} \cong 1.09$ W m^{-1} K^{-1}, and $\kappa_{\parallel}^{IJ1005} \cong 1.26$ W m^{-1} K^{-1}. Assuming these values for in-plane thermal conductivity of the printed films of the PEDOT:PSS studied here, the in-plane figures of merit, $z_{\parallel}T$, at room temperature are estimated to be $z_{\parallel}^{ICP1050}T \cong 1 \times 10^{-4}$, $z_{\parallel}^{PJ700}T \cong 3 \times 10^{-3}$, and $z_{\parallel}^{IJ1005}T \cong 2 \times 10^{-3}$. A comparison with the thermoelectric performance of other PEDOT-based formulations, limited to the cases in which only in-plane properties were combined,[23,27] reveals that the figure of merit of the commercially available PEDOT:PSS PJ700 is only slightly inferior to the in-plane figure of merit of ad hoc-prepared materials (0.005−0.008 at room temperature). Interestingly, the in-plane figure of merit is not an increasing function of the electrical conductivity, thus pointing out the need to better understand the effect of charge-carrier mobility and charge-carrier density on the thermoelectric properties of PEDOT:PSS.

The theoretical inverse proportionality between the thermopower $\alpha(T)$ and the electrical conductivity $\sigma(T)$ due to shifting of the Fermi level into the conduction band by doping was not observed: the increase of electrical conductivity from ICP1050 to PJ700 to IJ1005 is not correlated with a decrease in the thermopower, as PJ700 shows the highest value. This suggests that besides doping other variables play a role in the determination of these characteristics. The interdependencies between thermopower, doping, and mobility is described for degenerate systems by Mott's relation.[35] According to this

relation, and assuming a (semi)classical picture of the transport function, $\sigma(\varepsilon) = q\mu(\varepsilon)\, n(\varepsilon)$, the thermopower is a function of the energy dependence of the charge-carrier density, $n(\varepsilon)$, and mobility, $\mu(\varepsilon)$. In the formula

$$\alpha(T) = \frac{\pi^2 k_B^2 T}{3q} \frac{\partial \ln \sigma(\varepsilon)}{\partial \varepsilon}\bigg|_{\varepsilon=\varepsilon_F} \sim \frac{1}{q}\left(\frac{\partial \ln n(\varepsilon)}{\partial \varepsilon} + \frac{\partial \ln \mu(\varepsilon)}{\partial \varepsilon}\right)\bigg|_{\varepsilon=\varepsilon_F} \quad (4)$$

where the first term in brackets describes the dependence of thermopower on the shape of $n(\varepsilon)$ at the Fermi level, whereas the second term describes the dependence on the variation of charge-carrier mobility with respect to energy at the Fermi level. In particular, $\mu(\varepsilon)$ depends directly on energy but also indirectly by means of charge-carrier density; in fact, depending on the doping level, more or less energetic states of $n(\varepsilon)$ are occupied, thus giving access to states characterized by higher or lower mobility. Although the impact of the first term in brackets can be estimated from UPS measurements at the Fermi level,[20] the second term requires a batch of samples at different doping levels to be characterized, assuming that the morphology is unaffected by doping.[35] This latter assumption, although quite reasonable in conventional inorganic structures, is definitely not trivial in polymers, in which, for instance, doping by charge transfer from molecules could result in a modification of the morphology depending on the amount of volume occupied by such dopants.[10,44,49−51]

Mott's relation establishes a direct connection between the Seebeck coefficient and the shape of the density of states at the Fermi level when the dependency of the charge-carrier mobility on charge-carrier density is negligible, such as in the proven case of regioregular poly (3-hexylthiophene),[36] the mobility of which tends to saturate above a given amount of oxidation. Under this assumption, the second term in the brackets of eq 3 would be close to zero, and the shape of $n(\varepsilon)$ at the Fermi level would solely determine the absolute value of the thermopower.[4,5] It should be noted that whatever the absolute value of $n(\varepsilon)$ near the Fermi level, from Mott's relation, the same shapes of $n(\varepsilon)$ give the same contribution to the thermopower.

Since Mott's relation applies to degenerate systems only and because degeneracy of the formulations of PEDOT:PSS studied was demonstrated by recording the linear dependence of their thermopower with respect to temperature, Mott's relation should describe the formulations studied in this work. Therefore, UPS spectra were acquired with the aim to identify correlations between the measured thermopower and the corresponding $n(\varepsilon)$ at the Fermi level. The spectra taken from the representative PEDOT:PSS samples are shown in Figure 6.

The valence band spectrum is dominated by photoemission from the PSS units.[45] However, no signal close to the Fermi level is expected from PSS, and therefore the observation of the electronic structure responsible for the electrical and thermal conduction is possible irrespective of variations in the thickness of the superficial PSS layer, which could arise from different formulations and/or phase segregation.[45] The spectra shown in Figure 6a were all normalized to the photoemission intensity recorded at a BE of about 6 eV (the vertical dotted line in Figure 6a), following the strategy of O. Bubnova et al.[20] This particular normalization is not critical for the following discussion because it does not affect the shape of the photoemission spectra close to the Fermi level. The photoemission spectra are broadened as an

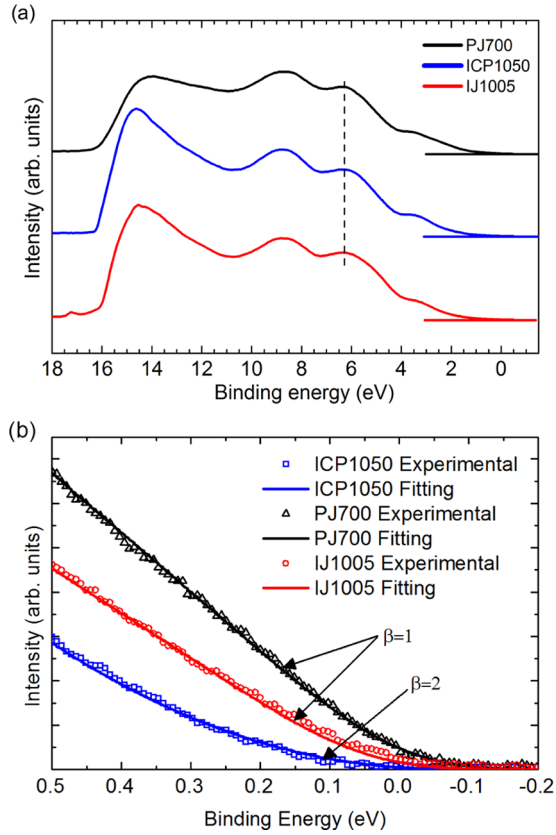

Figure 6. a) UPS spectra of the three PEDOT:PSS formulations investigated. (b) UPS spectra at the Fermi level (open symbols) and functional fittings (continuous lines). β is the exponent of the power law, $n(\varepsilon)$, chosen to fit the experimental data.

effect of the finite temperature of measurement and finite instrumental resolution. The former is accounted for by multiplying the density of states, $g(\varepsilon)$, by the Fermi function $f(\varepsilon) = \left[1 + \exp\left(\frac{\varepsilon - \varepsilon_F}{k_B T}\right)\right]^{-1}$, so that $n(\varepsilon) = g(\varepsilon)\, f(\varepsilon)$. The latter is modeled by a Gaussian distribution, $G(\varepsilon)$, to be convoluted with $n(\varepsilon)$ such that the spectra observed are given by intensity$(\varepsilon) = n(\varepsilon) \otimes G(\varepsilon)$. To extract the real shape of the charge-carrier density at the Fermi level, a very effective approach is thus to fit the acquired spectra with the convolution product. Supposing a power law shape for the density of states $g(\varepsilon) = A(\varepsilon - \varepsilon_F)^\beta$, the fitting function is

$$\text{intensity}(\varepsilon) = \frac{A(\varepsilon - \varepsilon_F)^\beta}{1 + \exp\left(\frac{\varepsilon - \varepsilon_F}{k_B T}\right)} \otimes \frac{1}{\sqrt{2\pi}\sum} \exp\left(-\frac{(\varepsilon - \varepsilon_F)^2}{2\sum^2}\right) \quad (5)$$

where ε is the energy, ε_F is the Fermi level, and $\sum$ is the standard deviation of the Gaussian distribution determining the resolution of the measurement. The standard deviation $\sum$ is related to the FWHM by $2.35\sum$ = FWHM, with FWHM = $\Delta\varepsilon_{instr} \cong 50$ meV. Then, $\sum$ results as equal to ≅22 meV. Close to the Fermi level (Figure 6b), the $n(\varepsilon)$ of both PJ700 and IJ1005 is well fitted by a linear density of states ($\beta = 1$), in agreement with what already observed in the literature,[45] whereas ICP1050 shows a quadratic behavior ($\beta = 2$). Therefore, if the thermopower was not affected

by mobility, PJ700 and IJ1005 that have the same shape of the $n(\varepsilon)$ at the Fermi level should have the same thermopower, and it would be higher than that of ICP1050, characterized by a quadratic shape. Instead, PJ700 is observed to have the highest thermopower, whereas ICP1050 and IJ1005 are approximately equal. Therefore, experimental differences among the measured thermopowers can be explained by Mott's relation only by supposing that the mobility term plays a role. To directly support this thesis, nontrivial mobility measurements would be required to study the energy-dependent mobility terms entering the transport function. Hall effect measurements, which are sensitive to the coherent fraction of charge carriers, have been recently shown of being insufficient on their own to study the charge-carrier mobility in disordered organic conductors, such as PEDOT:PSS.[52] On the other hand, by means of a morphology-independent electrostatic doping under the field-effect transistor configuration,[53,54] Wei et al. have recently demonstrated that charge-carrier mobility in highly conducting PEDOT:PSS depends on charge-carrier density for electrical conductivities, even up to hundreds of S/cm.[55] Their result supports the analysis made in this work, clearly pointing to the role played by mobility in the determination of the thermopower of PEDOT:PSS, even at high oxidation levels.

CONCLUSIONS

This work reported a detailed thermoelectric study of a set of highly conducting inkjet-printed films of commercially available PEDOT:PSS, characterized by different room-temperature electrical conductivities equal to 11.32 ± 1.57, 267.12 ± 4.05, and 462.86 ± 4.39 S/cm, respectively. The electronic transport mechanism of the least conductive formulation was found to be thermally activated across the full temperature range under investigation, from 260 to 420 K, whereas it shows a metal-like behavior above a certain critical temperature in the more conductive samples. The Seebeck coefficient, ranging from ≅14 μV K^{-1} (ICP1050, IJ1005) to 21 μV K^{-1} (PJ700), was found to be a linear function of temperature for all of the samples studied, irrespective of their transport mechanism, either thermally activated or metal-like, a typical behavior observed in degenerate systems. The cross-plane thermal conductivity measured with a scaling approach using a simplified pump−probe technique was found to be an increasing function of the in-plane electrical conductivity, that is, from 0.34 to 0.46 W m^{-1} K^{-1}. A first approximation estimate of the in-plane thermal conductivity, $\kappa_{\parallel}$, was extracted assuming validity of the Wiedemann−Franz law in the corresponding direction and $z_{\parallel}T$ values at room temperature were accordingly derived: a maximum value of 0.003 at room temperature was obtained, with samples characterized by an intermediate electrical conductivity.

To gain insights into the relation between the electronic structure of the polymer conductors under test and respective thermoelectric properties, Mott's relation was investigated using UPS spectroscopy to identify correlations between the shape of $n(\varepsilon)$ at the Fermi level and the thermopower. The shape of the acquired $n(\varepsilon)$ at the Fermi level and the measured thermopower were not found to be simply correlated, pointing to the critical role of charge carrier density-dependent mobility in the determination of the thermopower. The mutual dependency between the charge-carrier mobility and charge-carrier density is therefore a relevant factor in determining the thermopower even in highly conducting polymers, with electrical conductivities up to hundreds of S/cm, and it should be carefully assessed to rationalize the thermoelectric properties of organic conductors.

Overall, this work shows that the in-plane zT values in excess of ∼10^{-3} can be readily achieved in printed films obtained with off-the-shelf PEDOT:PSS formulations. A path toward cost-effective, large-area printing of polymer thermoelectric generators indicatively requires an improvement of this figure of merit of two orders of magnitude,[56] and a detailed understanding of the impact of mobility at varying charge densities in high-conducting formulations can provide fundamental indications to boost the thermoelectric properties of printable and largely available conducting polymers.

ASSOCIATED CONTENT

Supporting Information

The Supporting Information is available free of charge on the ACS Publications website at DOI: 10.1021/acsami.7b04533.

AFM images of the three formulations of PEDOT:PSS studied (PDF)

AUTHOR INFORMATION

Corresponding Author

*E-mail: mario.caironi@iit.it.

ORCID

Davide Beretta: 0000-0002-7739-7494
Alex J. Barker: 0000-0002-5614-4113
Gianlorenzo Bussetti: 0000-0001-8556-8014
Annamaria Petrozza: 0000-0001-6914-4537

Notes

The authors declare no competing financial interest.

ACKNOWLEDGMENTS

The preliminary stage of this research was financially supported by SAES GETTERS S.p.A.

REFERENCES

(1) Rowe, D. M. *Thermoelectrics Handbook: Macro to Nano*; Taylor & Francis: Boca Raton, 2006.

(2) Ziman, J. M.; Armstrong, H. L. Principles of the Theory of Solids. *Am. J. Phys.* **1965**, *33*, 349−350.

(3) Dresselhaus, M. S.; Chen, G.; Tang, M. Y.; Yang, R. G.; Lee, H.; Wang, D. Z.; Ren, Z. F.; Fleurial, J.-P.; Gogna, P. New Directions for Low-Dimensional Thermoelectric Materials. *Adv. Mater.* **2007**, *19*, 1043−1053.

(4) Hicks, L. D.; Dresselhaus, M. S. Effect of Quantum-Well Structures on the Thermoelectric Figure of Merit. *Phys. Rev. B: Condens. Matter Mater. Phys.* **1993**, *47*, 12727.

(5) Hicks, L. D.; Dresselhaus, M. S. Thermoelectric Figure of Merit of a One-Dimensional Conductor. *Phys. Rev. B: Condens. Matter Mater. Phys.* **1993**, *47*, 16631.

(6) Snyder, G. J.; Toberer, E. S. Complex Thermoelectric Materials. *Nat. Mater.* **2008**, *7*, 105−114.

(7) Søndergaard, R. R.; Hösel, M.; Espinosa, N.; Jørgensen, M.; Krebs, F. C. Practical Evaluation of Organic Polymer Thermoelectrics by Large-Area R2R Processing on Flexible Substrates. *Energy Sci. Eng.* **2013**, *1*, 81−88.

(8) Bubnova, O.; Khan, Z. U.; Malti, A.; Braun, S.; Fahlman, M.; Berggren, M.; Crispin, X. Optimization of the Thermoelectric Figure of Merit in the Conducting Polymer Poly (3, 4-Ethylenedioxythiophene). *Nat. Mater.* **2011**, *10*, 429−433.

(9) Schlitz, R. A.; Brunetti, F. G.; Glaudell, A. M.; Miller, P. L.; Brady, M. A.; Takacs, C. J.; Hawker, C. J.; Chabinyc, M. L. Solubility-Limited Extrinsic N-Type Doping of a High Electron Mobility Polymer for Thermoelectric Applications. *Adv. Mater.* **2014**, *26*, 2825−2830.

(10) Patel, S. N.; Glaudell, A. M.; Kiefer, D.; Chabinyc, M. L. Increasing the Thermoelectric Power Factor of a Semiconducting Polymer by Doping from the Vapor Phase. *ACS Macro Lett.* **2016**, *5*, 268−272.
(11) Chen, Y.; Zhao, Y.; Liang, Z. Solution Processed Organic Thermoelectrics: Towards Flexible Thermoelectric Modules. *Energy Environ. Sci.* **2015**, *8*, 401−422.
(12) Bounioux, C.; Díaz-Chao, P.; Campoy-Quiles, M.; Martín-González, M. S.; Goñi, A. R.; Yerushalmi-Rozen, R.; Müller, C. Thermoelectric Composites of poly(3-Hexylthiophene) and Carbon Nanotubes with a Large Power Factor. *Energy Environ. Sci.* **2013**, *6*, 918.
(13) Poehler, T. O.; Katz, H. E. Prospects for Polymer-Based Thermoelectrics: State of the Art and Theoretical Analysis. *Energy Environ. Sci.* **2012**, *5*, 8110−8115.
(14) Wuesten, J.; Ziegler, C.; Ertl, T. Electron Transport in Pristine and Alkali Metal Doped Perylene-3,4,9,10-Tetracarboxylicdianhydride (PTCDA) Thin Films. *Phys. Rev. B* **2006**, *74*, No. 125205.
(15) Gao, X.; Uehara, K.; Klug, D. D.; Tse, J. S. Rational Design of High-Efficiency Thermoelectric Materials with Low Band Gap Conductive Polymers. *Comput. Mater. Sci.* **2006**, *36*, 49−53.
(16) Pfeiffer, M.; Beyer, A.; Fritz, T.; Leo, K. Controlled Doping of Phthalocyanine Layers by Cosublimation with Acceptor Molecules: A Systematic Seebeck and Conductivity Study. *Appl. Phys. Lett.* **1998**, *73*, 3202.
(17) Aïch, R. B.; Blouin, N.; Bouchard, A.; Leclerc, M. Electrical and Thermoelectric Properties of Poly(2,7-Carbazole) Derivatives. *Chem. Mater.* **2009**, *21*, 751−757.
(18) Mateeva, N.; Niculescu, H.; Schlenoff, J.; Testardi, L. R. Correlation of Seebeck Coefficient and Electric Conductivity in Polyaniline and Polypyrrole. *J. Appl. Phys.* **1998**, *83*, 3111.
(19) Luo, J.; Billep, D.; Waechtler, T.; Otto, T.; Toader, M.; Gordan, O.; Sheremet, E.; Martin, J.; Hietschold, M.; Zahn, D. R. T.; Gessner, T. Enhancement of the Thermoelectric Properties of PEDOT:PSS Thin Films by Post-Treatment. *J. Mater. Chem. A* **2013**, *1*, 7576.
(20) Bubnova, O.; Khan, Z. U.; Wang, H.; Braun, S.; Evans, D. R.; Fabretto, M.; Hojati-Talemi, P.; Dagnelund, D.; Arlin, J.; Geerts, Y. H.; Desbief, S.; Breiby, D. W.; Andreasen, J. W.; Lazzaroni, R.; Chen, W. M.; Zozoulenko, I.; Fahlman, M.; Murphy, P. J.; Berggren, M.; Crispin, X. Semi-Metallic Polymers. *Nat. Mater.* **2014**, *13*, 190−194.
(21) Wei, Q.; Mukaida, M.; Kirihara, K.; Naitoh, Y.; Ishida, T. Recent Progress on PEDOT-Based Thermoelectric Materials. *Materials* **2015**, *8*, 732−750.
(22) Fabretto, M. V.; Evans, D. R.; Mueller, M.; Zuber, K.; Hojati-Talemi, P.; Short, R. D.; Wallace, G. G.; Murphy, P. J. Polymeric Material with Metal-Like Conductivity for Next Generation Organic Electronic Devices. *Chem. Mater.* **2012**, *24*, 3998−4003.
(23) Weathers, A.; Khan, Z. U.; Brooke, R.; Evans, D.; Pettes, M. T.; Andreasen, J. W.; Crispin, X.; Shi, L. Significant Electronic Thermal Transport in the Conducting Polymer poly(3,4-Ethylenedioxythiophene). *Adv. Mater.* **2015**, *27*, 2101−2106.
(24) Ionescu-Zanetti, C.; Mechler, A.; Carter, S. A.; Lal, R. Semiconductive Polymer Blends: Correlating Structure with Transport Properties at the Nanoscale. *Adv. Mater.* **2004**, *16*, 385−389.
(25) Nardes, A. M.; Kemerink, M.; Janssen, R. A. J. Anisotropic Hopping Conduction in Spin-Coated PEDOT: PSS Thin Films. *Phys. Rev. B: Condens. Matter Mater. Phys.* **2007**, *76*, No. 085208.
(26) Liu, J.; Wang, X.; Li, D.; Coates, N. E.; Segalman, R. A.; Cahill, D. G. Thermal Conductivity and Elastic Constants of PEDOT: PSS with High Electrical Conductivity. *Macromolecules* **2015**, *48*, 585−591.
(27) Wei, Q.; Mukaida, M.; Kirihara, K.; Ishida, T. Experimental Studies on the Anisotropic Thermoelectric Properties of Conducting Polymer Films. *ACS Macro Lett.* **2014**, *3*, 948−952.
(28) Nardes, A. M.; Janssen, R. A. J.; Kemerink, M. A Morphological Model for the Solvent-Enhanced Conductivity of PEDOT: PSS Thin Films. *Adv. Funct. Mater.* **2008**, *18*, 865−871.
(29) Zhou, J.; Anjum, D. H.; Chen, L.; Xu, X.; Ventura, I. A.; Jiang, L.; Lubineau, G. The Temperature-Dependent Microstructure of PEDOT/PSS Films: Insights from Morphological, Mechanical and Electrical Analyses. *J. Mater. Chem. C* **2014**, *2*, 9903−9910.
(30) Mengistie, D. A.; Chen, C.-H.; Boopathi, K. M.; Pranoto, F. W.; Li, L.-J.; Chu, C.-W. Enhanced Thermoelectric Performance of PEDOT:PSS Flexible Bulky Papers by Treatment with Secondary Dopants. *ACS Appl. Mater. Interfaces* **2015**, *7*, 94−100.
(31) Alemu, D.; Wei, H.-Y.; Ho, K.-C.; Chu, C.-W. Highly Conductive PEDOT:PSS Electrode by Simple Film Treatment with Methanol for ITO-Free Polymer Solar Cells. *Energy Environ. Sci.* **2012**, *5*, 9662.
(32) Park, T.; Park, C.; Kim, B.; Shin, H.; Kim, E. Flexible PEDOT Electrodes with Large Thermoelectric Power Factors to Generate Electricity by the Touch of Fingertips. *Energy Environ. Sci.* **2013**, *6*, 788.
(33) Sun, J.; Yeh, M. L.; Jung, B. J.; Zhang, B.; Feser, J.; Majumdar, A.; Katz, H. E. Simultaneous Increase in Seebeck Coefficient and Conductivity in a Doped Poly(alkylthiophene) Blend with Defined Density of States. *Macromolecules* **2010**, *43*, 2897−2903.
(34) Zhang, F.; Zang, Y.; Huang, D.; Di, C.; Gao, X.; Sirringhaus, H.; Zhu, D. Modulated Thermoelectric Properties of Organic Semiconductors Using Field-Effect Transistors. *Adv. Funct. Mater.* **2015**, *25*, 3004−3012.
(35) Cutler, M.; Mott, N. F. Observation of Anderson Localization in an Electron Gas. *Phys. Rev.* **1969**, *181*, 1336.
(36) Shimotani, H.; Diguet, G.; Iwasa, Y. Direct Comparison of Field-Effect and Electrochemical Doping in Regioregular Poly (3-Hexylthiophene). *Appl. Phys. Lett.* **2005**, *86*, No. 022104.
(37) Beretta, D.; Bruno, P.; Lanzani, G.; Caironi, M. Reliable Measurement of the Seebeck Coefficient of Organic and Inorganic Materials between 260 K and 460 K. *Rev. Sci. Instrum.* **2015**, *86*, No. 075104.
(38) Berti, G.; Calloni, A.; Brambilla, A.; Bussetti, G.; Duò, L.; Ciccacci, F. Direct Observation of Spin-Resolved Full and Empty Electron States in Ferromagnetic Surfaces. *Rev. Sci. Instrum.* **2014**, *85*, No. 073901.
(39) Capinski, W.; Maris, H.; Ruf, T.; Cardona, M.; Ploog, K.; Katzer, D. Thermal-Conductivity Measurements of GaAs/AlAs Superlattices Using a Picosecond Optical Pump-and-Probe Technique. *Phys. Rev. B* **1999**, *59*, 8105−8113.
(40) Cahill, D. G. Analysis of Heat Flow in Layered Structures for Time-Domain Thermoreflectance. *Rev. Sci. Instrum.* **2004**, *75*, 5119−5122.
(41) Shackelford, J. F.; Han, Y.-H.; Kim, S.; Kwon, S.-H. *CRC Materials Science and Engineering Handbook*, 4th ed.; Taylor & Francis: Boca Raton, 2015.
(42) Ioffe Institute, 2016. http://www.ioffe.ru/SVA/NSM/Semicond/ (accessed February, 2016).
(43) Hwang, J.; Amy, F.; Kahn, A. Spectroscopic Study on Sputtered PEDOT·PSS: Role of Surface PSS Layer. *Org. Electron.* **2006**, *7*, 387−396.
(44) Kim, G.-H.; Shao, L.; Zhang, K.; Pipe, K. P. Engineered Doping of Organic Semiconductors for Enhanced Thermoelectric Efficiency. *Nat. Mater.* **2013**, *12*, 719−723.
(45) Greczynski, G.; Kugler, T.; Keil, M.; Osikowicz, W.; Fahlman, M.; Salaneck, W. R. Photoelectron Spectroscopy of Thin Films of PEDOT − PSS Conjugated Polymer Blend: A Mini-Review and Some New Results. *J. Electron Spectrosc. Relat. Phenom.* **2001**, *121*, 1−17.
(46) Greczynski, G.; Kugler, T.; Salaneck, W. Characterization of the PEDOT-PSS System by Means of X-Ray and Ultraviolet Photoelectron Spectroscopy. *Thin Solid Films* **1999**, *354*, 129−135.
(47) Mott, N. F.; Davis, E. A. *Electronic Processes in Non-Crystalline Materials*, 2nd ed.; Oxford University Press: Oxford, 2012.
(48) Goldsmid, H. J. *Introduction to Thermoelectricity*; Springer Science & Business Media, 2009; Vol. *121*.
(49) Liu, C.; Jang, J.; Xu, Y.; Kim, H.-J.; Khim, D.; Park, W.-T.; Noh, Y.-Y.; Kim, J.-J. Effect of Doping Concentration on Microstructure of Conjugated Polymers and Characteristics in N-Type Polymer Field-Effect Transistors. *Adv. Funct. Mater.* **2015**, *25*, 758−767.
(50) Arkhipov, V. I.; Heremans, P.; Emelianova, E. V.; Bässler, H. Effect of Doping on the Density-of-States Distribution and Carrier Hopping in Disordered Organic Semiconductors. *Phys. Rev. B: Condens. Matter Mater. Phys.* **2005**, *71*, 1−7.

(51) Zuo, G.; Abdalla, H.; Kemerink, M. Impact of Doping on the Density of States and the Mobility in Organic Semiconductors. *Phys. Rev. B* **2016**, *93*, No. 235203.
(52) Kang, K.; Watanabe, S.; Broch, K.; Sepe, A.; Brown, A.; Nasrallah, I.; Nikolka, M.; Fei, Z.; Heeney, M.; Matsumoto, D.; Marumoto, K.; Tanaka, H.; Kuroda, S.; Sirringhaus, H. 2D Coherent Charge Transport in Highly Ordered Conducting Polymers Doped by Solid State Diffusion. *Nat. Mater.* **2016**, *15*, 892−902.
(53) Pernstich, K. P.; Rössner, B.; Batlogg, B. Field-Effect-Modulated Seebeck Coefficient in Organic Semiconductors. *Nat. Mater.* **2008**, *7*, 321−325.
(54) Warwick, C. N.; Venkateshvaran, D.; Sirringhaus, H. Accurate on-Chip Measurement of the Seebeck Coefficient of High Mobility Small Molecule Organic Semiconductors. *APL Mater.* **2015**, *3*, No. 096104.
(55) Wei, Q.; Mukaida, M.; Kirihara, K.; Naitoh, Y.; Ishida, T. Photoinduced Dedoping of Conducting Polymers: An Approach to Precise Control of the Carrier Concentration and Understanding Transport Properties. *ACS Appl. Mater. Interfaces* **2016**, *8*, 2054−2060.
(56) Beretta, D.; Perego, A.; Lanzani, G.; Caironi, M. Organic Flexible Thermoelectric Generators: From Modeling, a Roadmap towards Applications. *Sustainable Energy Fuels* **2017**, *1*, 174−190.